Nonconforming Schwarz-Spectral Element Methods For Incompressible Flow

Ketan Mittal, Som Dutta, Paul Fischer

Abstract

We present scalable implementations of spectral-element-based Schwarz overlapping (overset) methods for the incompressible Navier-Stokes (NS) equations. Our SEM-based overset grid method is implemented at the level of the NS equations, which are advanced independently within separate subdomains using interdomain velocity and pressure boundary-data exchanges at each timestep or sub-timestep. Central to this implementation is a general, robust, and scalable interpolation routine, *gslib-findpts*, that rapidly determines the computational coordinates (processor p, element number e, and local coordinates $(r, s, t) \in \hat{\Omega} := [-1, 1]^3$) for any arbitrary point $\mathbf{x}^* = (x^*, y^*, z^*) \in \Omega \subset \mathbb{R}^3$. The communication kernels in *gslib* execute with at most $\log P$ complexity for P MPI ranks, have scaled to $P > 10^6$, and obviate the need for development of any additional MPI-based code for the Schwarz implementation. The original interpolation routine has been extended to account for multiple overlapping domains. The new implementation discriminates the possessing subdomain by distance to the domain boundary, such that the interface boundary data is taken from the inner-most interior points. We present application of this approach to several heat transfer and fluid dynamic problems, discuss the computation/communication complexity and accuracy of the approach, and present performance measurements for $P > 12,000$.

Keywords: Overset, High-order, Scalability, Turbulence, Heat-Transfer

1. Introduction

High-order spectral element methods (SEMs) are well established as an effective means for simulation of turbulent flow and heat transfer in a variety of engineering applications (e.g., [1, 2, 3, 4]). Central to the performance and accuracy of these methods

*Mechanical Science and Engineering, University of Illinois at Urbana-Champaign

**CSI, City University of New York

Computer Science, University of Illinois at Urbana-Champaign

is the use of hexahedral elements, Ω^e, which are represented by isoparametric mappings of the reference element $\hat{\Omega} := [-1, 1]^d$ in d space dimensions. With such a configuration, it is possible to express all operators in a factored matrix-free form that requires only $O(n)$ storage, where $n = EN^d$ is the number of gridpoints for a mesh comprising E elements of order N. The fact that the storage scales as N^d and not N^{2d} is a major advantage of the spectral element method that was put forth in the pioneering work of Orszag [5] and Patera [6] in the early 80s. The work is also low, $O(N^{d+1})$, and can be cast as dense matrix-matrix products, which are highly efficient on modern-day architectures [1].

The efficiency and applicability of the SEM is tied closely to the ability to generate all-hex meshes for a given computational domain. While all-tet meshing is effectively a solved problem, the all-hex case remains challenging in many configurations. Here, we explore Schwarz overlapping methods as an avenue to support nonconforming discretizations in the context of the SEM. Overlapping grids simplify mesh generation by allowing the user to represent the solution on a complex domain as grid functions on relatively simpler overlapping regions (also known as *overset* or *chimera* grids). These simpler overlapping regions allow grid generation where local mesh topologies are otherwise incompatible, which is a feature of particular importance for complex 3D domains and in the simulation of flows in time-dependent domains subject to extreme mesh deformation. Overlapping grids also enable use of discretization of varying resolution in each domain based on the physics of the problem in that region.

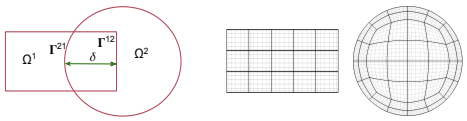

Figure 1: Overlapping rectangular and circular subdomains with corresponding spectral element meshes and Gauss-Lobatto-Legendre grids for $N = 7$. Γ^{ij} denotes the segment of the subdomain boundary $\partial\Omega^i$ that is interior to Ω^j.

Overlapping grids introduce a set of challenges that are not posed by a single conforming grid [7]. Using multiple meshes requires boundary condition for each *interface/artificial* boundary that is interior to the other domain (Γ^{12} and Γ^{21} in Fig. 1). Since these surfaces are not actual domain boundaries, boundary condition data must be interpolated from a donor element in the overlapping mesh, which must be identified at the beginning of a calculation. For moving or deforming meshes, donor elements must be re-identified after each timestep. Additionally, if multiple overlapping meshes share a target donor point, it is important to pick the donor mesh that will provide the most accurate solution. For production-level parallel computing applications, the identification of donor element, interpolation of data, and communication must be robust and scalable. Additionally, differences in resolution of the overlapping meshes can impact global mass-flux balances, leading to a violation of the divergence-free constraint with potentially stability consequences for incompressible flow calculations. These issues must be addressed in order to enable scalable and accurate turbulent flow and heat transfer calculations.

Since their introduction in 1983 [8], several overset methods have been developed for a variety of problems ranging from Maxwell's Equations [9] to fluid dynamics [10] to particle tracking [11]. Overset-grid methods are also included in commercial and research software packages such as Star-CCM [12], Overflow [13] and Overture [14]. Most of these implementations, however, are at most fourth-order accurate in space [9, 11, 15, 16, 17, 18]. Sixth-order finite-difference based methods have been presented in [19, 13], while sixth-order finite volume based schemes are available in elsA [20]. A spectral element based Schwarz method presented by Merrill et. al. [21] has demonstrated exponential convergence.

Here, we extend the work of Merrill et. al. [21] to develop a robust, accurate, and scalable framework for overlapping grids based on the spectral element method. We start with a brief description of the SEM and existing framework which we build upon (Section 2). We discuss our approach to fast, parallel, high-order interpolation of boundary data and a mass-balance correction that is critical for incompressible flow. Finally we present some applications in Section 3 which demonstrate the scalability and accuracy of our overlapping grid framework.

2. SEM-Schwarz for Navier-Stokes

The spectral element method (SEM) was introduced by Patera for the solution of the incompressible Navier-Stokes equations (NSE) in [6]. The geometry and the solution are represented using the Nth-order tensor-product polynomials on isoparametrically mapped elements. Variational projection operators are used to discretize the associated partial differential equations. While technically a Q_N finite element method (FEM), the SEM's strict matrix-free tensor-product formulation leads to fast implementations that are qualitatively different than classic FE methods. SE storage is only $O(n)$ and work scales as $O(EN^{d+1}) = O(nN)$, where $n = EN^d$ is the number of points for an E-element discretization of order N in $\mathbb{R}^d$. (Standard p-type FE formulations have work and storage complexities of $O(nN^d)$, which is prohibitive for $N > 3$.) All $O(N^{d+1})$ work terms in the SEM can be cast as fast matrix-matrix products. A central feature of the SEM is to use nodal bases on the Gauss-Lobatto-Legendre (GLL) points, which lead to an efficient and accurate (because of the high order) diagonal mass matrix. Overintegration (dealiasing) is applied only to the advection terms to ensure stability [22].

For the unsteady NSE, we use semi-implicit BDFk/EXTk timestepping in which the time derivative is approximated by a kth-order backward difference formula (BDFk), the nonlinear terms (and any other forcing) are treated with kth-order extrapolation (EXTk), and the viscous, pressure, and divergence terms are treated implicitly. This approach leads to a linear unsteady Stokes problem to be solved at each timestep, which is split into independent viscous and pressure (Poisson) updates, with the pressure-Poisson problem being the least well conditioned (and most expensive) substep in the time advancement. We support two spatial

discretizations for the Stokes problem: the $\mathbb{P}_N - \mathbb{P}_{N-2}$ formulation with a continuous Q_N velocity space and a discontinuous Q_{N-2} pressure space; and the $\mathbb{P}_N - \mathbb{P}_N$ approach having equal order continuous velocity and pressure. Full details are provided in [1, 23].

The Schwarz-SEM formulation of the NSE brings forth several considerations. Like all Schwarz methods, the basic idea is to interpolate data on subdomain boundaries that are interior to Ω from donor subdomains and to then solve the subdomain problems independently (in parallel) on different processor subsets. In principle, the NSE require only velocity boundary conditions. The first challenge is to produce that boundary data in an accurate and stable way. Spatial accuracy comes from using high-order (spectral) interpolation, as described in the next section.

For temporal accuracy, there are several new concerns. As a cost-saving measure, one can simply use lagged donor-velocity values (corresponding to piecewise-constant extrapolation) for the subdomain interface updates. While only first-order accurate, this scheme is stable without the need for subiterations. To realize higher-order accuracy (up to k), one can extrapolate the boundary data in time. Generally, this extrapolation must be coupled with a predictor-corrector iteration for the unsteady-Stokes substep. (The nonlinear term is already accurately treated by extrapolation and is stable provided one adheres to standard CFL stability limits.) Typically three to five subiterations (κ_{iter}) are needed per timestep to ensure stability [24] for mth-order extrapolation of the interface boundary data, when $m > 1$. Using this approach, Merrill *et al.* [21] demonstrated exponential convergence in space and up to third-order accuracy in time for Schwarz-SEM flow applications.

From a practical standpoint, our SEM domain decomposition approach is enabled by using separate MPI communicators for each overlapping mesh, Ω^s, which allows all of the existing solver technology (100K lines of code) to operate with minimal change. The union of these separate *session* (i.e., subdomain) communicators is `MPI_COMM_WORLD`, which is invoked for the subdomain data exchanges and for occasional collectives such as partition-of-unity-weighted integrals over $\Omega = \bigcup \Omega^s$. The data exchange and donor point-set identification is significantly streamlined through the availability of a robust interpolation library, *gslib-findpts*, which obviates the need for direct development of any new MPI code, as discussed next.

2.1. Interpolation

The centerpiece of our multidomain SEM-based nonconforming Schwarz code is the fast and robust interpolation utility *findpts*. This utility grew out of a need to support data interrogation and Lagrangian particle tracking on $P = 10^4$–10^6 processors. High fidelity interpolation for highly curved elements, like the ones supported by SEM, is quite challenging. Thus, *findpts* was designed with the principles of robustness (i.e., it should never fail) and speed (i.e., it should be fast).

findpts is part of *gslib*, a lightweight *C* communication package that readily links with any *Fortran*, *C*, or *C++* code. *findpts* provides two key capabilities. First, it

determines computational coordinates $\mathbf{q}^* = (e^*, p^*, r^*, s^*, t^*)$ (element e, processor p and reference-space coordinates $\mathbf{r} = (r, s, t)$) for any given point $\mathbf{x}^* = (x^*, y^*, z^*) \in \mathbb{R}^3$. Second, *findpts_eval* interpolates any given scalar field for a given set of computational coordinates (determined from *findpts*). Because interpolation is nonlocal (a point $\mathbf{x}^*$ may originate from any processor), *findpts* and *findpts_eval* require interprocessor coordination and must be called by all processors in a given communicator. For efficiency reasons, interpolation calls are typically batched with all queries posted in a single call, but the work can become serialized if all target points are ultimately owned by a single processor. All communication overhead is at most $\log P$ by virtue of *gslib*'s generalized and scalable[1] all-to-all utility, *gs_crystal*, which is based on the *crystal router* algorithm of [25].

To find a given point $\mathbf{q}^*(\mathbf{x}^*)$, *findpts* first uses a hash table to identify processors that could potentially own the target point $\mathbf{x}^*$. A call to *gs_crystal* exchanges copies of the $\mathbf{x}^*$ entries between sources and potential destinations. Once there, elementwise bounding boxes further discriminate against entries passing the hash test. At that point, a trust-region based Newton optimization is used to minimize $||\mathbf{x}^e(\mathbf{r}) - \mathbf{x}^*||^2$ and determine the computational coordinates for that point. The initial guess in the minimization is taken to be the closest point on the mapped GLL mesh for element e. In addition to returning the computational coordinates of a point, *findpts* also indicates whether a point was found inside an element, on a border, or was not found within the mesh. Details of the *findpts* algorithm are given in [26].

In the context of our multidomain Schwarz solver, *findpts* is called at the level of `MPI_COMM_WORLD`. One simply posts all meshes to *findpts_setup* along with a pair of discriminators. The first discriminator is an integer field which, at the setup and execute phases, is equal to the subdomain number (the *session id*). In the *findpts* setup phase, each element in Ω is associated with a single subdomain Ω^j, and the subdomain number j is passed in as the discriminator. During the *findpts* execute phase, one needs boundary values for interface points on Ω^j, but does not want these values to be derived from elements in Ω^j. All interface points associated with $\partial\Omega^j$ are tagged with the j discriminator and *findpts* will only search elements in $\Omega \backslash \Omega^j$.

In the case of multiply-overlapped domains, it is still possible to have more than one subdomain claim ownership of a given boundary point $\mathbf{x}^*$. To resolve such conflicts, we associate with each subdomain Ω^j a local distance function, $\delta^j(\mathbf{x})$, which indicates the minimum distance from any point $\mathbf{x} \in \Omega^j$ to $\partial\Omega^j$. The ownership of any boundary point $\mathbf{x}^* \in \partial\Omega^j$ between two or more domains Ω^k, $k \neq j$, is taken to be the domain that maximizes $\delta^k(\mathbf{x}^*)$. This choice is motivated by the standard Schwarz arguments, which imply that errors decay as one moves *away* from the interface, in accordance with decay of the associated Green's functions. We illustrate

[1] We note that `mpi_alltoall` is *not* scalable because its interface requires arguments of length P on each of P processors, which is prohibitive when $P > 10^6$.

this situation in Fig. 2.1 where $\mathbf{x}^* \in \partial\Omega^2$ belongs to Ω^1 and Ω^3. In this case, interpolated values (from *findpts_eval*) will come from Ω^1 because $\mathbf{x}^*$ is "more interior" to Ω^1 than Ω^3.

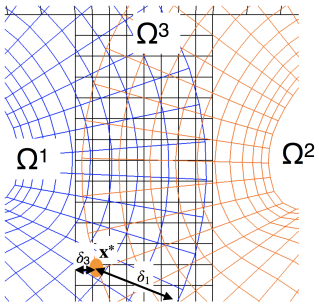

Figure 2: *findpts* considers distance from the interface boundaries (δ^1 in Ω^1 and δ^3 in Ω^3) when determining the best donor element for $\mathbf{x}^* \in \partial\Omega^2$.

2.2. Mass-Balance

Since pressure and divergence-free constraint are tightly coupled in incompressible flow, even small errors at interface boundaries (due to interpolation or use of overlapping meshes of disparate scales) can lead to mass-imbalance in the system, resulting in erroneous and unsmooth pressure contours. For a given subdomain Ω^j, the mass conservation statement for incompressible flow is simply

$$\int_{\partial\Omega^j} \mathbf{u}\cdot\hat{\mathbf{n}} \;=\; 0, \tag{1}$$

where $\hat{\mathbf{n}}$ represents the outward pointing unit normal vector on $\partial\Omega^j$. Our goal is to find a nearby correction to the interpolated surface data that satisfies (1).

Let $\partial\Omega_D$ denote the subset of the domain boundary $\partial\Omega$ corresponding to Dirichlet velocity conditions and $\partial\Omega_N$ be the Neumann (outflow) subset. If $\partial\Omega_N \cap \partial\Omega^j = 0$, then there is a potential to fail to satisfy (1) because the interpolated fluxes on $\partial\Omega^j$ may not integrate to zero. Let $\hat{\mathbf{u}}$ denote the tentative velocity field defined on $\partial\Omega^j$ through prescribed data on $\partial\Omega_d := \partial\Omega^j \cap \partial\Omega_D$ and interpolation on $\partial\Omega_i := \partial\Omega^j \backslash \partial\Omega_d$. Let $\mathbf{u} = \hat{\mathbf{u}} + \tilde{\mathbf{u}}$ be the flux-corrected boundary data on $\partial\Omega^j$ and $\tilde{\mathbf{u}}$ be the correction required to satisfy (1). One can readily show that the choice

$$\tilde{\mathbf{u}}|_{\partial\Omega_i} \;=\; \gamma\hat{\mathbf{n}}|_{\partial\Omega_i} \tag{2}$$

is the L^2 minimizer of possible trace-space corrections that allow (1) to be satisfied, provided that

$$\begin{aligned}\gamma \;&=\; -\frac{\int_{\partial\Omega_d}\hat{\mathbf{u}}\cdot\hat{\mathbf{n}}\,dA + \int_{\partial\Omega_i}\hat{\mathbf{u}}\cdot\hat{\mathbf{n}}\,dA}{\int_{\partial\Omega_i}\hat{\mathbf{n}}\cdot\hat{\mathbf{n}}\,dA} \\ &=\; -\frac{\int_{\partial\Omega^j}\hat{\mathbf{u}}\cdot\hat{\mathbf{n}}\,dA}{\int_{\partial\Omega_i}\hat{\mathbf{n}}\cdot\hat{\mathbf{n}}\,dA}.\end{aligned} \tag{3}$$

The denominator of (3) of course equates to the surface area of the interface boundary on Ω^j. The correction (2) is imposed every time boundary data is interpolated between overlapping domains during Schwarz iterations.

3. Results & Applications

We now present several applications that demonstrate the performance and accuracy of the Schwarz-SEM implementation.

3.1. Parallel Performance

A principal concern for the performance of Schwarz methods is the overhead associated with interpolation, especially for high-order

methods, where interpolation costs scale as $O(N^3)$ per interrogation point in $\mathbb{R}^3$. Our first examples address this question.

Figure 3 shows a test domain consisting of a single spectral element ($N = 15$) in $\mathbb{R}^3$. The spiral configuration leads to many local mimima in the Newton functional, but the use of nearest GLL points as initial guesses generally avoids being trapped in false minima. On a 2.3 GHz Macbook Pro, *findpts* requires ≈ 0.08 seconds to find $\mathbf{q}$ for 1000 randomly distributed points on $\hat{\Omega}$ to a tolerance of 10^{-14}.

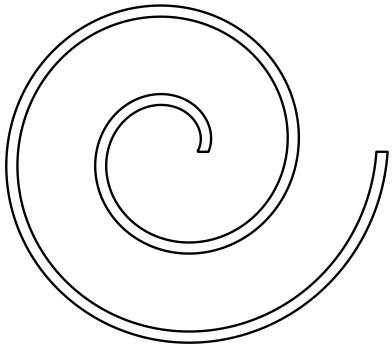

Figure 3: 2D slice of a 3D spiral at $N = 15$. *findpts* robustly finds 1000 random points in ≈ 0.08 sec.

In addition to the *findpts* cost, we must be concerned with the overhead of the repeated *findpts_eval* calls, which are invoked once per subiteration for each Schwarz update. In a parallel setting, interpolation comes with the additional overhead of communication, which is handled automatically in $\log P$ time by *findpts_eval*. Figure 4 shows a strong-scale plot of time versus number of processors P for a calculation with E=20,000 spectral elements at $N = 7$ (n=6.8 million grid points) on Cetus, an IBM Blue Gene/Q at the Argonne Leadership Computing Facility. For this geometry, shown in Fig. 5, there are 2000 elements at the interface-boundary with a total of 128,000 interface points that require interpolation at each Schwarz iteration. Overlapping domains simplify mesh generation for this problem by allowing an inner mesh (twisting in the spanwise direction) to overlap with an extruded outer mesh.

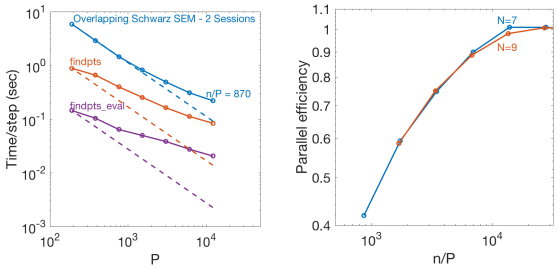

Figure 4: (left) Strong scaling plot at $N = 7$, and (right) parallel efficiency of the method at $N = 7$ and $N = 9$.

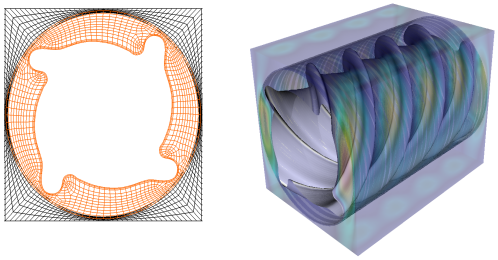

Figure 5: (left) Overlapping 2D spectral element meshes for the notched-cylinder geometry, and (right) velocity magnitude contours highlighting the twisted cylinder.

Figure 4 shows scaling for overall time per step and time spent in *findpts* and *findpts_eval*. Due to the inherent load imbalance in overlapping grids, owing to the fact that all interface elements might not be located on separate processors, the scaling for *findpts*

and *findpts_eval* is not ideal. However, *findpts* takes only 10% and *findpts_eval* takes 1% of time compared to the total time to solution per timestep, and as a result the scaling of the overall method is maintained. The parallel efficiency of the calculation is more than 90% until the number of MPI ranks exceeds the number of interface elements. The parallel efficiency drops to 60% at $n/P = 1736$, which is in accord with performance models for the (monodomain) SEM [27].

3.2. Exact Solution for Decaying Vortices

Our next example demonstrates that the Schwarz implementation preserves the exponential convergence expected of the SEM. Walsh derived a family of exact eigenfunctions for the Stokes and Navier-Stokes equations based on a generalization of Taylor-Green vortices in the periodic domain $\Omega = [0, 2\pi]^2$. For all integer pairs (m, n) satisfying $\lambda = -(m^2 + n^2)$, families of eigenfunctions can be formed by defining streamfunctions ψ that are linear combinations of $\cos(mx)\cos(ny)$, $\sin(mx)\cos(ny)$, $\cos(mx)\sin(ny)$, and $\sin(mx)\sin(ny)$.Taking as an initial condition the eigenfunction $\hat{\mathbf{u}} = (-\psi_y, \psi_x)$, a solution to the NSE is $\mathbf{u} = e^{\nu\lambda t}\hat{\mathbf{u}}(\mathbf{x})$. The solution is stable only for modest Reynolds numbers. Interesting long-time solutions can be realized, however, by adding a relatively high-speed mean flow to the eigenfunction. We demonstrate the multidomain capability using the three meshes illustrated in Fig. 6 (left); a periodic background mesh has a square hole in the center while a pair of circular meshes cover the hole.

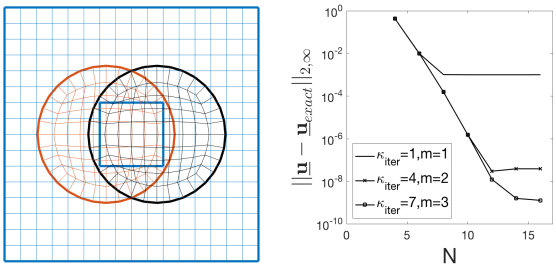

Figure 6: Walsh Eddy Problem: (left) three overlapping spectral element meshes and (right) spectral convergence for error in velocity.

Exponential convergence of the velocity error with respect to N is demonstrated in Fig. 6 (right). (Here, the norm is the pointwise maximum of the 2-norm of the vector field, i.e., $||\underline{\mathbf{e}}||_{2,\infty} := \max_i ||\mathbf{e}_i||_2$.) For extrapolation orders $m = 1$, 2, and 3, κ_{iter} was set to 1, 4 and 7 to ensure stability.

3.3. Vortex Breakdown

Escudier [28] studied vortex breakdown in a cylindrical container with a lid rotating at angular velocity Ω. He considered cylinders for various different H/R i.e. height to radius ratio, at different $Re = \frac{\Omega^2 R}{\nu}$. Sotiropoulos & Ventikos [29] did a computational study on this experiment comparing the structure and location of the bubbles that form as a result of vortex breakdown. Here, we use overlapping grids for $Re = 1854$ and $H/R = 2$ case to compare our results against [28], [29], and a monodomain SEM based solution. The monodomain mesh has 140 elements at $N = 9$. The overlapping mesh was generated by cutting the monodomain across the cylinder axis and extruding the two halves. The calculations were run with $m = 1$ and $\kappa_{iter} = 1$

(no subiteration) for 2000 convective time-units to reach steady state. Figure 7 compares the axial velocity along the centerline for monodomain and overlapping grids based solution, and Table 1 compares these solution with Escudier and Sotiropoulos. At this resolution, the Schwarz-SEM and SEM results agree to within < 1 percent and to within 1 to 2 percent of the results of [29].

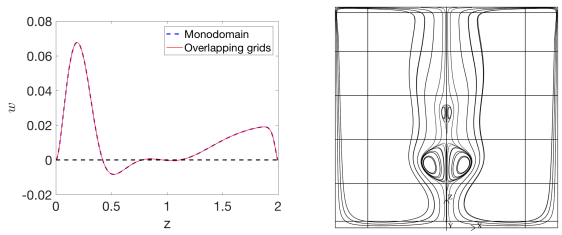

Figure 7: Vortex breakdown problem: (left) w along cylinder centerline and (right) in-plane streamlines.

	z_1	z_2	z_3	z_4
Overlapping	0.4222	0.7752	0.9596	1.1186
Monodomain	0.4224	0.7748	0.9609	1.1191
Escudier	0.42	0.74	1.04	1.18
Sotiropoulos	0.42	0.772	0.928	1.09

Table 1: Zero-crossings (z) for vertical velocity along cylinder centerline for the vortex breakdown.

3.4. Turbulent Channel Flow

Turbulent boundary layers are one of the applications where overlapping grids offer the potential for significant savings. These flows feature fine scale structures near the wall with relatively larger scales in the far-field. As a first step to addressing this class of problems, we validate our Schwarz-SEM scheme for turbulent channel flow, for which abundant data is available in literature. In particular, we compare mono- and multidomain SEM results at Reynolds number $Re_\tau = \frac{u_\tau h}{\nu} = 180$ with direct numerical simulation (DNS) results of Moser et. al. [30], who used 2.1 million grid points, and with the DNS of Vreman & Kuerten [31], which used 14.2 million grid-points. The Reynolds number is based on the friction velocity u_τ at the wall, channel half-height h and the fluid kinematic viscosity ν, with $u_\tau = \sqrt{\frac{\tau_w}{\rho}}$ determined using the wall shear stress τ_w and the fluid density ρ.

Table 2 lists the key parameters for the four different calculations. Following [30] and [31], the streamwise and spanwise lengths of the channel were $4\pi h$ and $4\pi h/3$, respectively. Statistics for all SEM results were collected over 50 convective time units.

	Re_τ	Ω_y	Grid-size
Monodomain	179.9	$[-1, 1]$	$18\times18\times18\times N^3$
Overlapping	179.9	$[-1, -0.88]$ $[-0.76, 1]$	$19\times4\times19\times N^3$ $18\times15\times18\times N^3$
Moser	178.1	$[-1, 1]$	$128 \times 129 \times 128$
Vreman	180	$[-1, 1]$	$384 \times 193 \times 192$

Table 2: Parameters for channel flow calculations.

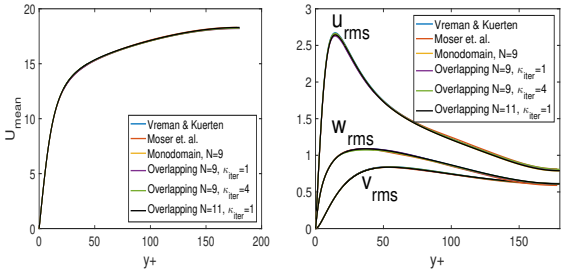

Figure 8: Comparison of monodomain, overlapping grid, and Moser et. al. with Vreman & Kuerten for U_{mean} (left) and u_{rms}, v_{rms} and w_{rms} at $N = 7$ and $N = 9$.

Figure 8 shows the mean streamwise velocity (U_{mean}) and fluctuations (u_{rms}, v_{rms} and w_{rms}) versus $y^+ = \frac{u_\tau y}{\nu}$ for each case, where y is the distance from the nearest wall. For the

Schwarz case, several combinations of resolution (N) and subiteration counts (κ_{iter}) were considered. We quantify the relative error for each quantity by computing the norm of the relative percent difference from the results of Vreman & Kuerten. Specifically, define

$$\epsilon_\psi(y) \quad := \quad 100\frac{\psi(y) - \psi(y)_{Vreman}}{\psi(y)_{Vreman}} \qquad (4)$$

and

$$||\epsilon_\psi|| \quad := \quad \frac{1}{2h}\int_{-h}^{h} \epsilon_\psi \, dy \qquad (5)$$

for each quantity $\psi = U_{mean}$, u_{rms}, v_{rms} and w_{rms} in Table 3. All statistics are within one percent of the results of [31]. The results indicate that increasing the number of Schwarz iterations and resolution leads to better comparison, as expected.

	U_{mean}	u_{rms}	v_{rms}	w_{rms}
Monodomain, $N = 9$	0.17	1.00	0.60	0.57
Monodomain, $N = 11$	0.16	0.46	0.49	0.71
Overlapping, $N = 9$, $\kappa_{iter} = 1$, $m = 1$	0.43	1.69	0.89	0.77
Overlapping, $N = 9$, $\kappa_{iter} = 4$, $m = 3$	0.21	0.92	0.60	1.05
Overlapping, $N = 11$, $\kappa_{iter} = 1$, $m = 1$	0.17	1.58	0.74	0.31
Moser et. al.	0.04	0.15	0.52	1.62

Table 3: Relative % difference for channel flow results compared with Vreman & Kuerten [31].

3.5. Heat Transfer Enhancement

The effectiveness of wire-coil inserts to increase heat transfer in pipe flow has been studied through an extensive set of experiments by Collins *et al.* at Argonne National Laboratory [32]. Monodomain spectral element simulations for this configuration based on 2D meshes that were extruded and twisted were described in [33]. Here, we consider an overlapping mesh approach pictured in Fig. 9, in which a 2D mesh is extruded azimuthally with a helical pitch. The singularity at the pipe centeriline is avoided by using a second (overlapping) mesh to model the central flow channel. The overlapping mesh avoids the topological constraint of mesh conformity and leads to better mesh quality. Mesh smoothing [34] further improves the conditioning of the system for the pressure Poisson equation. This approach also allows us to consider noncircular (e.g., square) casings, which are not readily accessible with the monodomain approach. As a first step towards these more complex configurations, we validate our Schwarz-SEM method with this real-world turbulent heat transfer problem.

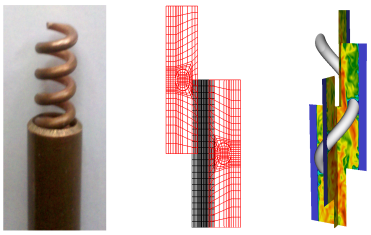

Figure 9: (left) Wire-coil insert [32], (center) overlapping spectral element meshes, and (right) velocity magnitude contours.

Here, we present results from calculations for two different pitches of the wire-coil insert to demonstrate the accuracy of our method. The geometric parameters were $e/p = 0.0940$ (long-pitch) and $e/p = 0.4273$ (optimal-pitch), with $e/D = 0.2507$, where e and p are the respective wire diameter and pitch and D is the inner diameter of the pipe. The Reynolds number of the flow is $UD/\nu = 5300$ and the Prandtl number is 5.8. Figure 9

shows a typical wire-coil insert (left), overlapping meshes used to discretize the problem (center), and a plot of velocity magnitude for flow at $Re = 5300$ (right).

For $e/p = 0.0940$, the Nusselt number Nu was determined to be 100.25 by experimental calculation, 112.89 by the monodomain calculation, and 113.34 by the overlapping-grid calculation. For $e/p = 0.4273$, Nu was determined to be 184.25 by the experiment, and 186 by the overlapping-grid calculation. The overlapping grid calculations were spatially converged and used $\kappa_{iter} = 4$ and $m = 3$. Figure 10 shows a slice of the velocity and temperature contours for the optimal pitch calculation.

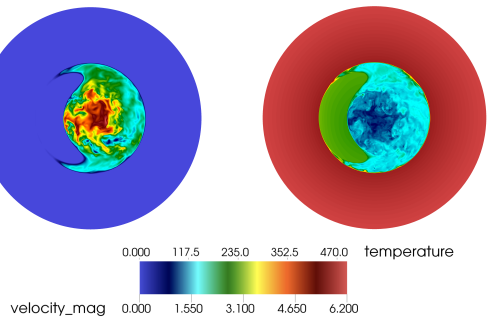

Figure 10: Velocity magnitude (left) and temperature slice of the wire-coil insert of optimal pitch.

4. Conclusion

We have presented a scalable Schwarz-SEM method for incompressible flow simulation. Use of an extended *gslib-findpts* library for donor-element identification and for data interpolation obviated the need for direct development of MPI code, even in the presence of multiple overlapping meshes. Strong scaling tests show that the parallel performance meets theoretical expectations. We have introduced mass-flux corrections to ensure divergence-free flow, even in the presence of interpolation error. We demonstrated exponential convergence for the method and showed excellent agreememnt in several complex three-dimensional flow configurations.

5. Acknowledgments

This work was supported by the U.S. Department of Energy, Office of Science, the Office of Advanced Scientific Computing Research, under Contract DE-AC02-06CH11357. An award of computer time on Blue Waters was provided by the National Center for Supercomputing Applications. Blue Waters is a sustained-petascale HPC and is a joint effort of the University of Illinois at Urbana-Champaign and its National Center for Supercomputing Applications. The Blue Waters sustained-petascale computing project is supported by the National Science Foundation (awards OCI-0725070 and ACI-1238993) and the state of Illinois. This research used resources of the Argonne Leadership Computing Facility, which is a DOE Office of Science User Facility.

6. References

References

[1] M. O. Deville, P. F. Fischer, E. H. Mund, High-order methods for incompressible fluid flow, Vol. 9, Cambridge University Press, 2002.

[2] S. Dutta, P. Fischer, M. H. Garcia, Large Eddy Simulation (LES) of flow and bedload transport at an idealized 90-degree diversion: Insight into Bulle effect, River Flow 2016: Iowa City, USA, July 11-14, 2016 (2016) 101.

[3] S. M. Hosseini, R. Vinuesa, P. Schlatter, A. Hanifi, D. S. Henningson, Direct numerical simulation of the flow around a wing section at moderate reynolds number, International Journal of Heat and Fluid Flow 61 (2016) 117–128.

[4] E. Merzari, A. Obabko, P. Fischer, Spectral element methods for liquid metal reactors applications, arXiv preprint arXiv:1711.09307.

[5] S. A. Orszag, Spectral methods for problems in complex geometrics, in: Numerical methods for partial differential equations, Elsevier, 1979, pp. 273–305.

[6] A. T. Patera, A spectral element method for fluid dynamics: laminar flow in a channel expansion, Journal of computational Physics 54 (3) (1984) 468–488.

[7] W. Chan, R. Gomez, Rogers se, buning pg. best practices in overset grid generation. aiaa# 2002-3191, in: 32nd Fluid Dynamics Conference, St. Louis MI, 2002.

[8] J. L. Steger, F. C. Dougherty, J. A. Benek, A chimera grid scheme.[multiple overset body-conforming mesh system for finite difference adaptation to complex aircraft configurations].

[9] J. B. Angel, J. W. Banks, W. D. Henshaw, A high-order accurate fdtd scheme for maxwell's equations on overset grids, in: Applied Computational Electromagnetics Society Symposium (ACES), 2018 International, IEEE, 2018, pp. 1–2.

[10] D. D. Chandar, B. Boppana, V. Kumar, A comparative study of different overset grid solvers between openfoam, starccm+ and ansys-fluent, in: 2018 AIAA Aerospace Sciences Meeting, 2018, p. 1564.

[11] A. Koblitz, S. Lovett, N. Nikiforakis, W. Henshaw, Direct numerical simulation of particulate flows with an overset grid method, Journal of Computational Physics 343 (2017) 414–431.

[12] S.-C. CD-adapco, V7. 02.008, User Manual.

[13] R. H. Nichols, P. G. Buning, Users manual for overflow 2.1, University of Alabama and NASA Langley Research Center.

[14] F. Bassetti, D. Brown, K. Davis, W. Henshaw, D. Quinlan, Overture: an object-oriented framework for high performance scientific computing, in: Proceedings of the 1998 ACM/IEEE conference on Supercomputing, IEEE Computer Society, 1998, pp. 1–9.

[15] J. G. Coder, D. Hue, G. Kenway, T. H. Pulliam, A. J. Sclafani, L. Serrano, J. C. Vassberg, Contributions to the sixth drag prediction workshop using structured, overset grid methods, Journal of Aircraft (2017) 1–14.

[16] W. D. Henshaw, A fourth-order accurate method for the incompressible navier-stokes equations on overlapping grids, Journal of computational physics 113 (1) (1994) 13–25.

[17] M. J. Brazell, J. Sitaraman, D. J. Mavriplis, An overset mesh approach for 3d mixed element high-order discretizations, Journal of Computational Physics 322 (2016) 33–51.

[18] J. A. Crabill, J. Sitaraman, A. Jameson, A high-order overset method on moving and deforming grids, in: AIAA Modeling and Simulation Technologies Conference, 2016, p. 3225.

[19] J. Aarnes, N. Haugen, H. Andersson, High-order overset grid method for detecting particle impaction on a cylinder in a cross flow, arXiv preprint arXiv:1805.10039.

[20] L. Cambier, S. Heib, S. Plot, The onera elsa cfd software: input from research and feedback from industry, Mechanics & Industry 14 (3) (2013) 159–174.

[21] B. E. Merrill, Y. T. Peet, P. F. Fischer, J. W. Lottes, A spectrally accurate method for overlapping grid solution of incompressible navier–stokes equations, Journal of Computational Physics 307 (2016) 60–93.

[22] J. Malm, P. Schlatter, P. F. Fischer, D. S. Henningson, Stabilization of the spectral element method in convection dominated flows by recovery of skew-symmetry, Journal of Scientific Computing 57 (2) (2013) 254–277.

[23] P. Fischer, M. Schmitt, A. Tomboulides, Recent developments in spectral element simulations of moving-domain problems, in: Recent Progress and Modern Challenges in Applied Mathematics, Modeling and Computational Science, Springer, 2017, pp. 213–244.

[24] Y. T. Peet, P. F. Fischer, Stability analysis of interface temporal discretization in grid overlapping methods, SIAM Journal on Numerical Analysis 50 (6) (2012) 3375–3401.

[25] G. Fox, W. Furmanski, Hypercube algorithms for neural network simulation: the crystal_accumulator and the crystal router, in: Proceedings of the third conference on Hypercube concurrent computers and applications: Architecture, software, computer systems, and general issues-Volume 1, ACM, 1988, pp. 714–724.

[26] A. Noorani, A. Peplinski, P. Schlatter, Informal introduction to program structure of spectral interpolation in nek5000.

[27] P. F. Fischer, Scaling limits for pde-based simulation, in: 22nd AIAA Computational Fluid Dynamics Conference, 2015, p. 3049.

[28] M. Escudier, Observations of the flow produced in a cylindrical container by a rotating endwall, Experiments in fluids 2 (4) (1984) 189–196.

[29] F. Sotiropoulos, Y. Ventikos, Transition from bubble-type vortex breakdown to columnar vortex in a confined swirling flow, International journal of heat and fluid flow 19 (5) (1998) 446–458.

[30] R. D. Moser, J. Kim, N. N. Mansour, Direct numerical simulation of turbulent channel flow up to re τ= 590, Physics of fluids 11 (4) (1999) 943–945.

[31] A. Vreman, J. G. Kuerten, Comparison of direct numerical simulation databases of turbulent channel flow at re τ= 180, Physics of Fluids 26 (1) (2014) 015102.

[32] J. T. Collins, C. M. Conley, J. N. Attig, M. M. Baehl, Enhanced heat transfer using wire-coil inserts for high-heat-load applications., Tech. rep., Argonne National Lab., IL (US) (2002).

[33] A. Y. Goering, Numerical investigation of wire coil heat transfer augmentation, Ph.D. thesis (2016).

[34] K. Mittal, P. Fischer, Mesh smoothing for the spectral element method, Journal of Scientific Computing (2018) 1–22.